



## REST Journal on Emerging trends in Modelling and Manufacturing

Vol: 11(1), March 2025

REST Publisher; ISSN: 2455-4537 (Online)

Website: <https://restpublisher.com/journals/jemm/>

DOI: <https://doi.org/10.46632/jemm/11/1/4>



# A Novel Photo Voltaic Inverter Topology with ANFIS Based MPPT for Maximum Power Extraction and Multilevel Inverter Integration

\*P. Abdul Raheem Khan, Sake Jaya Prakash, Syed Umaima, Khaiski Patan Anjum, K. S. Sai Kumar, Bandela Siva Krishna.

Annamacharya Institute of Technology & Sciences (Autonomous) Kadapa, Andhra Pradesh, India.

\*Corresponding Author Email: [abdulraheem.p25@gmail.com](mailto:abdulraheem.p25@gmail.com)

**Abstract:** This paper presents a novel photovoltaic (PV) inverter topology designed for maximum solar power utilization, which incorporates a new maximum power point tracking (MPPT) scheme based on shading pattern identification using an Adaptive Neuro-Fuzzy Inference System (ANFIS) controller. The proposed topology features a Single-Input Multi-Output (SIMO) converter and a Multilevel Inverter (MLI) to optimize energy conversion efficiency. Under partially shaded conditions, the ANFIS-based MPPT controller effectively tracks the maximum power point by analyzing the shading pattern, ensuring the PV system extracts maximum power. The SIMO converter then processes the PV voltage and generates four independent voltages ( $V_1$ ,  $V_2$ ,  $V_3$ , and  $V_4$ ) of varying magnitudes. The MLI subsequently converts the DC output voltage of the SIMO converter into a high-quality AC voltage suitable for grid integration, with a reduced harmonic distortion profile. The MLI consists of eight switching devices and is capable of producing a 31-level AC output voltage with minimal harmonic distortion. A key feature of the proposed system is the robust MPPT performance under varying weather conditions, coupled with the efficiency of the MLI in feeding the utility grid. An experimental prototype has been developed, with an FPGA Spartan trainer kit used to program the necessary control pulses for the MLI and SIMO converter, demonstrating the effectiveness of the proposed PV inverter topology.

## 1. INTRODUCTION

Nowadays, electric power generation through PV systems has emerged as an alternative to conventional power generating systems due to simple maintenance, eco-friendly nature, low noise and abundant availability. Extracting maximum power and inverting the output power of the PV system into useful ac to feed the utility are the tedious task associated with solar power generation. In order to extract maximum solar power, Maximum Power Point (MPP) of the PV system has to be tracked continuously using a Maximum Power Point Tracking (MPPT) controller [1]. In recent times, miniature range installation of solar power generating units on building rooftops is trending and also offers as an alternative primary source of energy for household purposes during emergence [2], [3]. In [4], presented the two Perturb and Observe (P&O) implementation technique based on the parameters like voltage and duty ratio and both the algorithm are applied to the solar pumping system. During dynamic weather conditions, voltage based algorithm performance is affected due to low pass filter noise at the same time duty ratio based P&O algorithm fails to track power path perfectly. A hybrid P&O scheme is presented in [5], still the response time of the scheme affects the performance. In [6], the performance of the traditional P&O is enhanced by improving a free running loop using Particle Swarm Optimization (PSO). Due to the involvement of metaheuristic algorithms, the proposed scheme is not suggested for low cost applications. During the change in irradiance there exists drift in the power curve, in order to eliminate the drift a new resolution is introduced into the system based on the panel current [7]. Due to excess feedback, the controller takes much time to decide MPP during regular conditions [8]. To feed the utility grid DC power generated from the PV array has to be inverted into AC power. Generally, the conversion circuit includes a dc-dc power converter and Multi-Level Inverter (MLI) [9]. To avoid voltage mismatch between PV source and DC voltage bus a dc-dc converter is incorporated such that low-level PV voltage is boosted up to the voltage level of DC bus. In continuation the boosted DC solar power is converted into AC power using inverters [10]. To reduce wastage of power, PV array and power conversion circuit efficiency should be high. From the past few years, many researchers have designed MLI with increased voltage levels having better

conversion efficiency with reduced harmonic content and minimum interface to electromagnetic interface [11], [12]. Traditional MLI configurations such as diode-clamped and flying capacitors topologies generate several voltage levels using capacitor circuits. The major problems associated with these two configurations are it is not possible to regulate the voltage across the capacitors. Moreover, conversion efficiency decreases as the voltage level is increased. Cascade H-bridge is much suitable to develop several voltage levels by employing asymmetric voltage technology, but these converters require more switching devices. In [13], experimentally implemented a novel topology to minimize DC offset voltage during unbalance and fault tolerant conditions. As the rating of the topology increases, it is difficult to control voltage across the capacitor. Hence, this topology is limited for off-grid applications. During low irradiance level, PV system produces the low voltage. To improve the efficiency of inverter during low voltage He and Cheng [14] developed a new multilevel inverter based on bridge modular switched capacitor. The configuration involves the number of switching devices and practical implementation of the control circuit is complex [15], [16]. Agrawal and Jain [17] presented a new MLI from the existing cross-connected source based inverter with a reduced number of switches by developing a simple control circuit to integrate low/medium/high voltages extracted from renewable energy sources to the grid. Under dynamic weather conditions, the proposed topology has poor performance. The above limitations associated with the existing scheme gives scope for the development of a novel PV inverter topology.

## 2. PV INVERTER TOPOLOGY

In order to generate thirty-one levels in the output voltage of the conventional cascaded H-bridge [18] MLI, it requires fifteen independent voltage sources and sixty power electronic switches. Lee et al. [19] presented modified H-bridge MLI with same thirty-one levels in the output voltage. Still the modified configuration requires four dc voltage sources and sixteen electronic switches. In view of the above limitations this project presents a novel PV inverter topology for maximum solar power utilization, which consists of PV system, dc-dc Single Input and Multi Output power converter and a simple thirty-one level inverter with the reduced number of switches as shown in Fig. 1. The PV system is employed with a novel MPPT controller based on shading pattern identification using artificial neural network to harvest maximum available solar power from RNG 200D 200Watt PV panel in any weather condition. The dc-dc Single Input and Multi-Output (SIMO) power converter incorporate a step-up converter with a transformer. The SIMO converter provides four independent output voltages V1, V2, V3 and V4 with different magnitudes. Finally, it is worth to mention that the thirty-one level inverter generates a sinusoidal waveform that is in phase with the utility grid using the four independent output voltages of the SIMO converter with unity power factor [20].

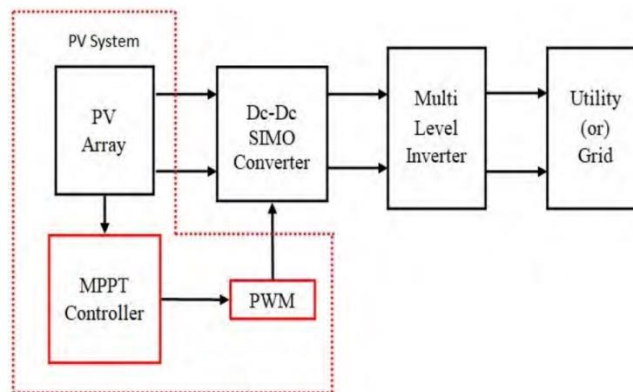


FIGURE 1. Schematic diagram of the proposed topology

**Proposed MPPT Scheme:** Conventional MPPT schemes fail to accomplish Global Maximum Power Point (GMPP) of the PV system during Partial Shaded Conditions (PSC) at the same time meta heuristic algorithms developed to track GMPP are complex, costly and require much time to track GMPP. Therefore, it is significant to develop a new optimizing algorithm for GMPP tracking under PSC, which has better accuracy, improved convergence time, simple to implement and moreover economical [21].

**Mathematical Modelling of PV System:** Due to obstacles such as passing clouds, shadows of buildings, dust deposit on panels and bird's waste it is not possible to receive uniform irradiance all over the system. Hence, effective irradiance (GE) on each PV module varies and it can be given as

$$G_E = (1 - S)G$$

where G is irradiance on un-shaded areas, S is the shading ratio of the panel. Shading ratio is defined as the ratio of shaded area on the module to total area of the module. Output current of the PV module is given as

$$I = I_{Ph} - I_D \left[ \exp \left( \frac{q(V_{PV} + I_{PV}R_S)}{N_S A B_K T} \right) - 1 \right] - \frac{V_{PV} + I_{PV}R_S N_S}{N_S R_{Sh}}$$

where IPh is photo generated current (A), ID is diode saturation current (A), VPV is panel voltage (V), IPV is p current (A), RS is series resistance (•), NS is number of PV cell connected in series, A is diode ideality factor, BK is Boltzmann constant, T is temperature on the panel (°C) and RSh is parallel resistance (•). Photo generated current with shaded and un-shaded cells can be written individually as

$$\left. \begin{aligned} I_{Ph(G_1)} &= (I_{SC,Ref} + K_{ISC} (T - T_{Ref})) \frac{G_1}{G_{Ref}} \\ I_{Ph(G_2)} &= (I_{SC,Ref} + K_{ISC} (T - T_{Ref})) \frac{G_2}{G_{Ref}} \\ I_{Ph(G_3)} &= (I_{SC,Ref} + K_{ISC} (T - T_{Ref})) \frac{G_3}{G_{Ref}} \\ I_{Ph(G_4)} &= (I_{SC,Ref} + K_{ISC} (T - T_{Ref})) \frac{G_4}{G_{Ref}} \end{aligned} \right\}$$

where IPh(G1), IPh(G2), IPh(G3) and IPh(G4) is photo generated current with respect to the irradiance on the panel surface (A), KISC is current coefficient, ISC,Ref is short circuit current at Standard Test Conditions (STC) (A), TRef is temperature at STC (°C), GRef is irradiance at STC (W/m<sup>2</sup>), G1, G2, G3 and G4 is irradiance on individual panels (W/m<sup>2</sup>), For a 2S2P configuration under PSC, PV system output current and voltage are expressed as

$$\left. \begin{aligned} I_{PV} &= \text{Min}(I_1, I_2, I_3, I_4) \\ V_{PV} &= V_1 + V_2 + V_3 + V_4 \end{aligned} \right\}$$

where I1 I2, I3 and I4 are panel currents that are calculated by substituting IPh(G1), IPh(G2), IPh(G3) and IPh(G4) in Eq. (3). In general, if the PV system has ‘n’ number of modules connected in series, the output current and voltage under PSC can be expressed as

$$\begin{aligned} \text{If } I_{PV} > I_{Ph(n-1)} \\ I_{PV} &= I_{Ph}(G_n) - I_D \left[ \exp \left( \frac{q(V_n + I_{PV}R_S)}{N_S A B_K T} \right) - 1 \right] - \frac{V_n + I_{PV}R_S N_S}{N_S R_{Sh}} \end{aligned} \tag{5a}$$

$$V_{PV} = V_n$$

$$\begin{aligned} \text{If } I_{Ph(n-2)} < I_{PV} < I_{Ph(n-1)} \\ I_{PV} &= I_{Ph}(G_{n-1}) - I_D \left[ \exp \left( \frac{q(V_{n-1} + I_{PV}R_S)}{N_S A B_K T} \right) - 1 \right] - \frac{V_{n-1} + I_{PV}R_S N_S}{N_S R_{Sh}} \end{aligned} \tag{6a}$$

$$V_{PV} = V_n + V_{n-1}$$

Similarly if,  $I_{PV} < I_{Ph1}$

$$I_{PV} = I_{Ph}(G_1) - I_D \left[ \exp \left( \frac{q(V_1 + I_{PV}R_S)}{N_S A B K T} \right) - 1 \right] - \frac{V_1 + I_{PV}R_S N_S}{N_S R_{Sh}}$$

$$V_{PV} = V_1 + V_2 + \dots + V_n$$

During partial shaded condition, total power (PT) of PV system is

$$P_T = P_1(G_{E1}) + P_2(G_{E2}) + \dots + P_n(G_{En})$$

where  $E_1, E_2, \dots, E_n$  are the effective irradiances of the PV modules.

**1.ANFIS:** The Adaptive Neuro-Fuzzy Inference System (ANFIS) is an intelligent system that integrates the benefits of two powerful methodologies: Fuzzy Logic Systems and Neural Networks. Fuzzy logic is used to model uncertainty and imprecision in systems, while neural networks are used to learn from data and adjust system parameters to minimize errors. ANFIS combines these to form a robust approach for modelling and controlling nonlinear systems that involve uncertainty, such as weather-driven systems in energy conversion and power management.

**2.Structure of ANFIS:** ANFIS combines both fuzzy inference systems and neural networks. The architecture of ANFIS is typically organized into five layers, each with a specific function. The layers interact to map inputs to outputs while adapting based on training.

**2.1 Layer 1: Fuzzification Layer**

The fuzzification layer is responsible for converting crisp inputs into fuzzy values using **membership functions**. Each node in this layer corresponds to a membership function for the input variable. For instance, if the input is temperature, its fuzzy membership functions could include "Low," "Medium," and "High." For an input  $x$ , the output of each node is calculated using a membership function:

$$O_{i1} = \mu_{A_i}(x)$$

Where:

- $O_i$  is the output of the  $i$ -th node in Layer 1.
- $\mu_{A_i}(x)$  is the membership function associated with the  $i$ -th fuzzy set for the input  $x$ .
- 

**2.2 Layer 2: Rule Layer**

In this layer, fuzzy rules are applied. Each node represents a fuzzy rule, which combines the fuzzy inputs to compute the degree of rule applicability. The output of this layer is the product of the incoming signals, representing the degree of firing of each rule.

For two inputs  $x$  and  $y$  with membership functions  $\mu_{A_i}(x)$  and  $\mu_{B_j}(y)$ , the output of the  $ij$ -th node in Layer 2 is given by:

$$O_{ij2} = w_{ij} = \mu_{A_i}(x) \cdot \mu_{B_j}(y)$$

Where  $w_{ij}$  is the firing strength of the rule.

**2.3 Layer 3: Normalization Layer**

In this layer, the firing strengths of each rule are normalized to ensure that the total weight is equal to 1. This normalization step is critical for combining rule outputs and ensuring a balanced decision-making process.

The output of each node in this layer is calculated as:

$$O_{ij3} = \frac{w_{ij}}{\sum_{i,j} w_{ij}}$$

Where  $w_{ij}$  is the firing strength from Layer 2, and the denominator is the sum of all firing strengths.

#### 2.4 Layer 4: Defuzzification Layer

In this layer, the output of each rule is calculated by multiplying the normalized firing strengths with the consequent parameters of the fuzzy rules. The output is the weighted output for each rule.

If the fuzzy rule is of the form:

$$\text{IF } x \text{ is } A_i \text{ AND } y \text{ is } B_j \text{ THEN } z = p_{ij}x + q_{ij}y + r_{ij}$$

Where  $p_{ij}$ ,  $q_{ij}$ , and  $r_{ij}$  are the parameters associated with the consequent part of the fuzzy rule.

#### 2.5 Layer 5: Output Layer

The final layer computes the overall output of the system. It is simply the sum of all the weighted outputs from Layer 4:

This output corresponds to the crisp output value that the system computes based on the fuzzy rules and the input data.

$$O_5 = \sum_{i,j} O_{ij4}$$

This output corresponds to the crisp output value that the system computes based on the fuzzy rules and the input data.

### 3. Mathematical Analysis of ANFIS Training

The key challenge in ANFIS is optimizing the fuzzy system's parameters (the membership function parameters and the consequent parameters of the rules) to minimize the error between predicted and actual outputs. ANFIS uses a combination of gradient descent and least squares methods to achieve this optimization.

#### 3.1 Error Minimization in ANFIS

To minimize the error between the actual output  $y^k$  and the predicted output  $\hat{y}^k$ , ANFIS uses a **backpropagation algorithm** to adjust the parameters. The error is typically defined as the mean squared error:

$$E = \frac{1}{N} \sum_{k=1}^N (\hat{y}_k - y_k)^2$$

Where:

- $\hat{y}_k$  is the predicted output for the  $k$ -th data point.
- $y_k$  is the actual output for the  $k$ -th data point.
- $N$  is the number of data points.

#### 3.2 Gradient Descent for Parameter Optimization

The parameters of the membership functions and fuzzy rules are optimized using gradient descent. The algorithm adjusts the parameters iteratively to reduce the error function:

$$\theta_{ij} = \theta_{ij} - \eta \cdot \frac{\partial E}{\partial \theta_{ij}}$$

Where  $\theta_{ij}$  represents the parameters of the system (either the fuzzy membership function parameters or the consequent parameters), and  $\eta$  is the learning rate.

#### 3.3 Least Squares for Consequent Parameters

The parameters of the consequent part of the fuzzy rules (e.g.,  $p_{ij}$ ,  $q_{ij}$ , and  $r_{ij}$ ) are optimized using least squares estimation, which minimizes the sum of squared errors between the predicted and actual output values.

### Application of ANFIS in Maximum Power Point Tracking (MPPT)

In the context of photovoltaic (PV) systems, Maximum Power Point Tracking (MPPT) is an essential technique used to extract the maximum power from solar panels under varying conditions (e.g., partial shading, temperature changes, etc.). ANFIS can play a pivotal role in improving the efficiency of MPPT algorithms.

#### 4.1 MPPT Problem in PV Systems

A solar panel's output power is highly dependent on the irradiance and temperature. Under partial shading conditions, traditional MPPT algorithms may fail to track the global maximum power point (GMPP) due to the existence of multiple local maxima. ANFIS, by dynamically adjusting to the changing conditions of shading, can provide more accurate MPPT tracking.

#### ANFIS for MPPT

For MPPT, ANFIS uses inputs like solar irradiance, temperature, and voltage as features. The network learns from these inputs to predict the maximum power point more effectively. Using the rules of fuzzy logic, ANFIS can handle uncertainty and noise in environmental data, ensuring better tracking even when the weather conditions are unpredictable. The output of the ANFIS controller determines the duty cycle for the converter that adjusts the operating point of the solar panel to the maximum power point. The Adaptive Neuro-Fuzzy Inference System (ANFIS) offers a powerful solution to problems involving uncertainty and nonlinear behaviour, as seen in applications such as Maximum Power Point Tracking (MPPT) for photovoltaic systems. By combining the strengths of fuzzy logic and neural networks, ANFIS provides a robust framework that can learn from data while maintaining interpretability through fuzzy rules. Its ability to model complex, dynamic systems under varying conditions makes it an ideal tool for optimizing energy harvesting in renewable energy systems. Through its training process, ANFIS adjusts its parameters to minimize errors and continuously adapt to changes in input data, ensuring improved performance in real-time applications like solar energy conversion.

**MLI with Reduced Switch Count:** In this topology, full bridge converter is connected in cascade to the diode as shown in Fig. 3. Inverter operation is explained in two parts, (a) positive cycle and (b) negative cycle.  $V_1$ ,  $V_2$ ,  $V_3$  and  $V_4$  voltages of the converter are constant and made equal to 6V, 12V, 24V and 48V.

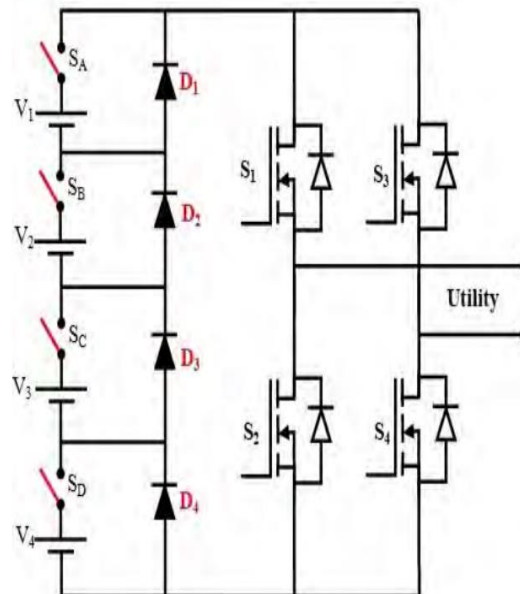


FIGURE 3. Thirty one level inverter configuration.

**Inverter Operation in The Positive Cycle:** For ease of analysis, positive cycle operation is further divided into sixteen modes. During the entire positive cycle mode of operation, full bridge converter switches  $S_1$  and  $S_2$  are in on-state. Mode 1: In this mode of operation, the switch  $S_A$  is in on-state and the rest of the switches are in off-state as shown in Fig. 4(a). At this point, inverter output voltage is equal to  $V_1$  i.e., 6V. Mode 2: In this mode of operation the switch  $S_B$  is in on-state, therefore  $D_1$  is forward bias and the remaining diodes are reverse biased, hence the voltage path is through  $D_1$  as shown in Fig. 4(b). At this point, inverter output voltage is 12V. Mode 3: Fig. 4(c) shows the operation of the inverter. During this mode of operation  $S_A$  and  $S_B$  switches are turned on. At this particular mode,  $V_1$  and  $V_2$  voltages are added, the output voltage across the inverter will be 18V. Mode 4: During this mode of operation the switch  $S_C$  is closed and the voltage path is through forward biased  $D_1$  and  $D_2$  diodes as shown in Fig. 4(d). The output voltage of the inverter will be 24V. Mode 5: The switches  $S_A$  and  $S_C$  are closed, in this situation the diode  $D_2$  is forward biased and the rest of the diodes are reverse biased. The voltage

path is clearly shown in Fig. 4(e). The output voltage across the inverter will be 30V. Mode 6: In this mode of operation, the switches SB and SC are in on-state as shown in Fig. 4(f). Both the voltages V2 and V3 are added to obtain an output voltage of 36V across the inverter.

Mode 7: During this mode of operation, switches SA, SB and SC are closed such that the voltage V1, V2 and V3 are added to give a total voltage of 42V as the output of the inverter. The switching states and voltage path is clearly shown in the Fig. 4(g).

**TABLE 1.** Switching states of the power electronic devices (L- voltage levels, V-voltage).

L	V	S <sub>A</sub>	S <sub>B</sub>	S <sub>C</sub>	S <sub>D</sub>	S <sub>1</sub>	S <sub>2</sub>	S <sub>3</sub>	S <sub>4</sub>
1	90V	on	on	on	on	on	off	off	on
2	84V	off	on	on	on	on	off	off	on
3	78V	on	off	on	on	on	off	off	on
4	72V	off	off	on	on	on	off	off	on
5	66V	on	on	off	on	on	off	off	on
6	60V	off	on	off	on	on	off	off	on
7	54V	on	off	off	on	on	off	off	on
8	48V	off	off	off	on	on	off	off	on
9	42V	on	on	on	off	on	off	off	on
10	36V	off	on	on	off	on	off	off	on
11	30V	on	off	on	off	on	off	off	on
12	24V	off	off	on	off	on	off	off	on
13	18V	on	on	off	off	on	off	off	on
14	12V	off	on	off	off	on	off	off	on
15	6V	on	off	off	off	on	off	off	on
16	0V	off	off	off	off	on	off	off	on
17	-6V	on	off	off	off	off	on	on	off
18	-12V	off	on	off	off	off	on	on	off
19	-18V	on	on	off	off	off	on	on	off
20	-24V	off	off	on	off	off	on	on	off
21	-30V	on	off	on	off	off	on	on	off
22	-36V	off	on	on	off	off	on	on	off
23	-42V	on	on	on	off	off	on	on	off
24	-48V	off	off	off	on	off	on	on	off
25	-54V	on	off	off	on	off	on	on	off
26	-60V	off	on	off	on	off	on	on	off
27	-66V	on	on	off	on	off	on	on	off
28	-72V	off	off	on	on	off	on	on	off
29	-78V	on	off	on	on	off	on	on	off
30	-84V	off	on	on	on	off	on	on	off
31	-90V	on	on	on	on	off	on	on	off

Mode 8: The switch SD is in on-state, in this situation D1, D2 and D3 diodes are forward biased. Respective voltage path in this mode of operation is shown in Fig. 4(h). Therefore output voltage across the inverter will be 48V.

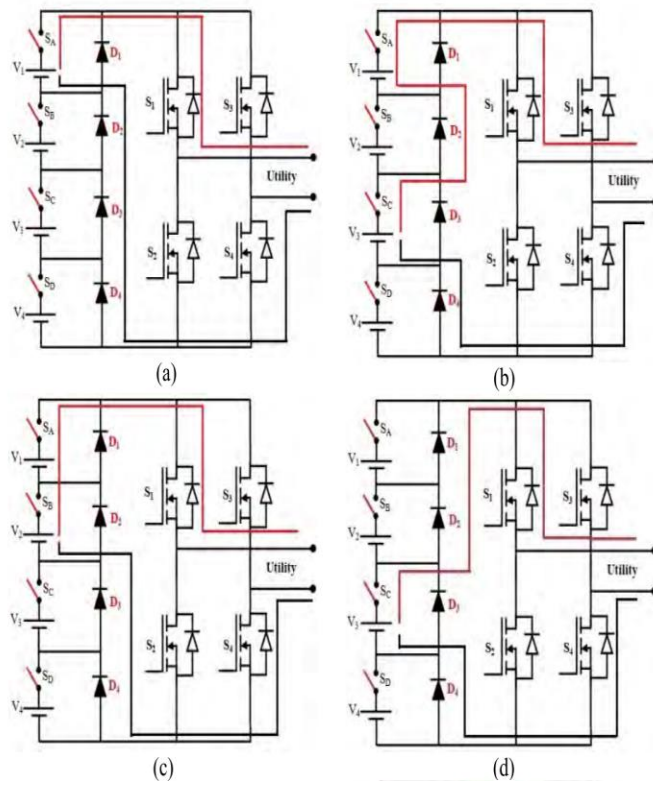


**FIGURE 4.** Operating Modes of Inverter during Positive Half Cycle (a) Mode 1, (b) Mode 2, (c) Mode 3, (d) Mode 4

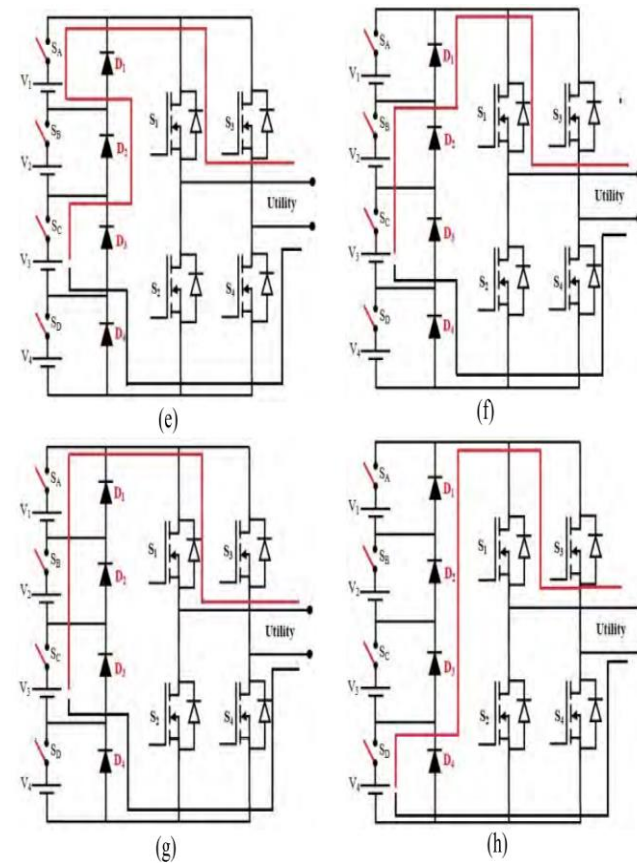


**FIGURE 5.** Operating Modes of Inverter during Positive Half Cycle (e) Mode 5, (f) Mode 6, (g) Mode 7 and (h) Mode 8.

Mode 9: During this mode of operation, the switch SA and SD are in on-state as shown in Fig. 4(i). The diodes D2 and D3 are forward biased, therefore the voltages V1 and V4 are accumulated to obtain a voltage of 54V across

the inverter. Mode 10: In this mode of operation, switches SB and SD are closed as shown in Fig. 4(j). As the diode D3 is forward biased both the voltage V2 and V4 are added and hence the output voltage of the inverter is 60V. Mode 11: The switches SA, SB and SD are closed as shown in Fig. 4(k). Due to this switching sequence, D3 diode gets forward bias and hence all the three voltages V1, V2 and V4 are added to get a 66V output voltage across the inverter. Mode 12: In this mode of operation, the switch SC and SD are in on-state as shown in Fig. 4(l). Therefore this switching phenomenon results in inverter output voltage as 72V. The voltage path is through D1 and D2 diodes, which are forward biased. Mode 13: During this mode of operation, the switches SA, SC and SD are closed as shown in Fig. 4(m). As the D2 diode gets forward bias all the three voltages are added. In this situation output voltage of the inverter will be 78V. Mode 14: In the Fig. 4(n) operation of the inverter is depicted. From Fig, it is clear that the switches SB, SC and SD are closed these results forward bias of the diode D1. As the switches SB, SC and SD are in on-state, the output voltage of the inverter will be 84V. Mode 15: In this mode of operation all the four switches are closed as shown in Fig. 4(o). The final output voltage of the inverter will be 90V. Mode 16: During this mode of operation, all the four switches are opened as shown in Fig. 4(p). The output voltage of the inverter is equal to 0V.

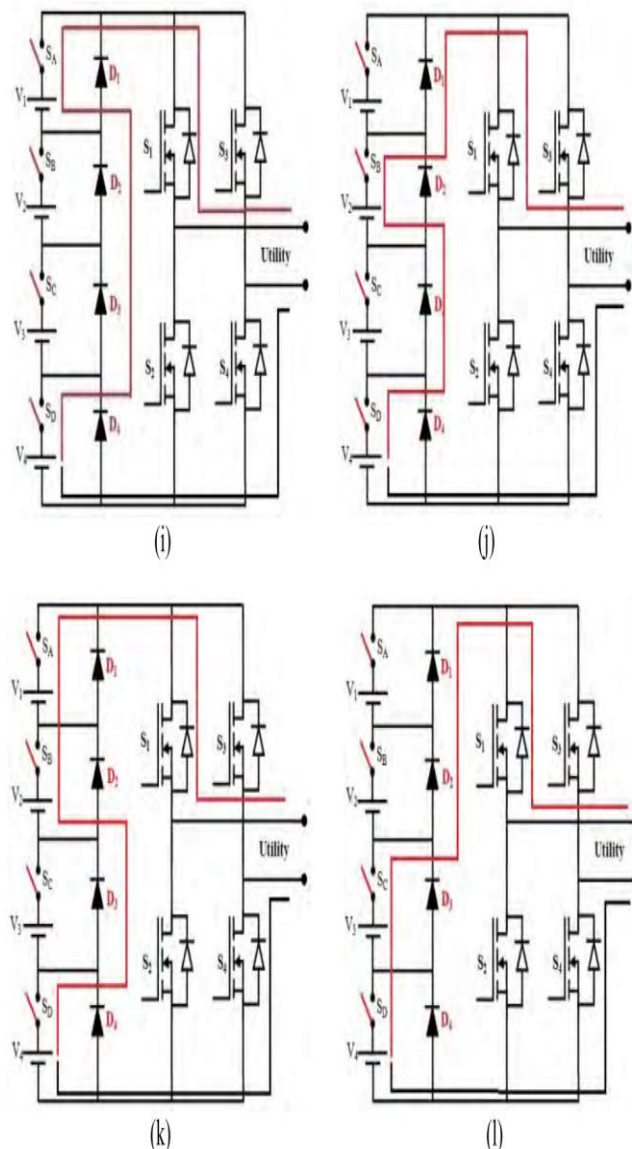


**FIGURE 6.** (Continued) Operating Modes of Inverter during Positive Half Cycle (i) Mode 9, (j) Mode 10, (k) Mode 11, (l) Mode 12

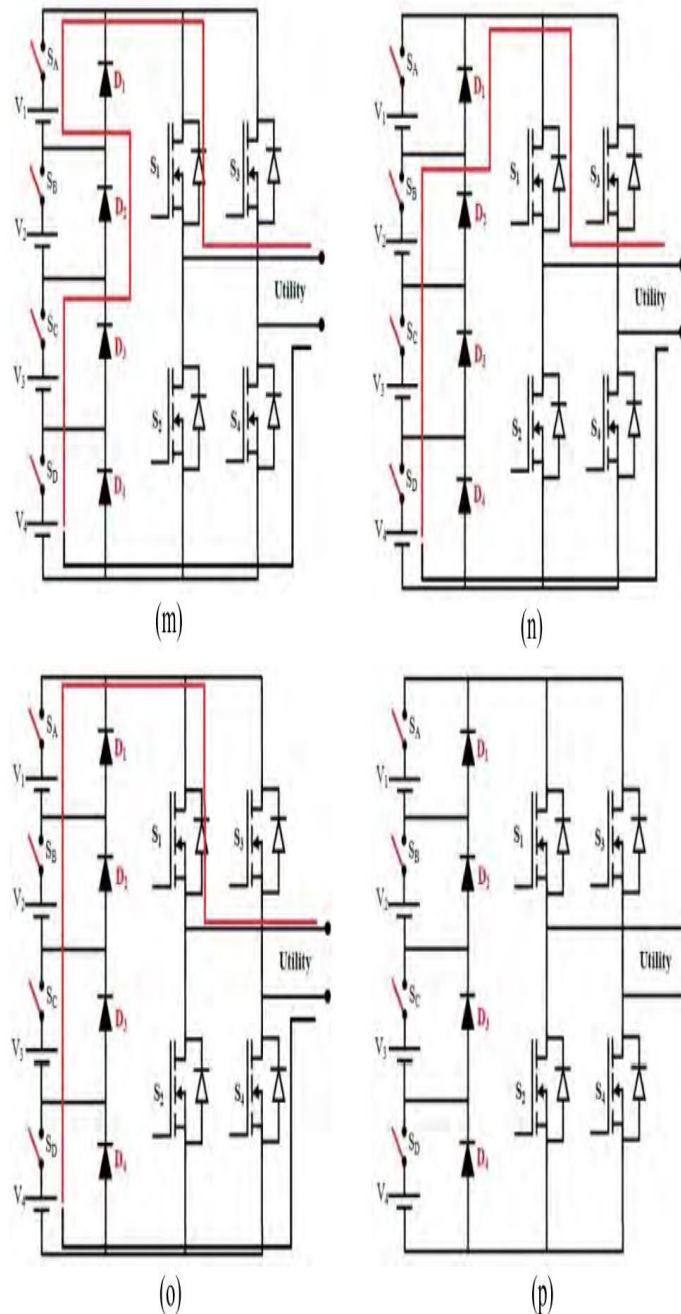


**FIGURE 7.** (Continued) Operating Modes of Inverter during Positive Half Cycle (m) Mode 13, (n) Mode 12, (o) Mode 15 and (p) Mode 16

Finally, inverter output voltages for the positive cycle in the sixteen modes of operation are 6V, 12V, 18V, 24V, 30V, 36V, 42V, 48V, 54V, 60V, 66V, 72V, 78V, 84V, 90V and 0V respectively.

**Inverter Operation in The Negative Cycle:** Similar, to the positive cycle the operation of the negative cycle is illustrated in sixteen modes. In the negative cycle, the output voltage of the inverter is same as that of the positive cycle. Furthermore, only switches S2 and S3 of the full bridge converter are operated. Output voltage of the inverter during negative cycle are -6V, -12V, -18V, -24V, -30V, -36V, -42V, -48V, -54V, -60V, -66V, -72V, -78V, -84V, -90V and 0V. The final summary of both the cycles can be given as 90V, 84V, 78V, 72V, 66V, 60V, 54V, 48V, 42V, 36V, 30V, 24V, 18V, 12V, 6V, 0V, -6V, -12V, -18V, -24V, -30V, -36V, -42V, -48V, -54V, -60V, -66V, -72V, -78V, -84V and -90V. Current Mode Controller (CMC) is used to control thirty-one level inverter. Pulse Width Modulation (PWM) technique is employed to generate control signals to the power electronic switches. As there is a change in the utility voltage, inverter output voltage has to be changed with respect to utility voltage. The proposed thirty-one level inverter topology has only eight power electronic switches. Hence, compared with the traditional multilevel inverters the proposed topology is simple to implement. Switching states of the power electronic devices are tabulated in Table 1.

### 3. SIMULATION RESULTS

Initially, the proposed GMPPT scheme is tested at Standard Test Conditions. Fig. 5 shows the performance of 2S2P configuration (a) output power, (b) output current and (c) output voltage. From figure, it is clear that till irradiance pattern is decided and MPP voltage is provided transients are observed. Once duty cycle of the converter is obtained, maximum solar power is extracted with reduced oscillations. As the tools employed in the MPPT scheme are direct mapping tools in between input and target data, very little percentage of oscillations are observed. Under standard test conditions, the proposed MPPT scheme has extracted maximum power from the PV system with reduced oscillations. During solar power generation partial shading phenomenon is unavoidable. Hence, testing at STC can't justify the effectiveness of the MPPT scheme. Therefore the performance of the proposed MPPT scheme is examined under PSC. GMPPT tracking ability of the proposed MPPT scheme is examined under different shading patterns using 2S2P configurations. Using MATLAB/Simulink different shading patterns are developed and named in number. At a time, duration of 0.2sec, shading patterns are changed from one to other respectively. As discussed earlier, till irradiance pattern and required MPP voltage is decided by the MPPT scheme transient oscillations are observed. But the transient oscillations are very little as of the direct mapping tools are involved to obtain target input. Similarly, for the rest of patterns the proposed GMPPT scheme has tracked the exact power path during partial shading conditions. The actual power for the respective patterns is indicated by the black graph. Similarly, red colour represents obtained power using the proposed MPPT scheme. Therefore the proposed GMPPT scheme has tracked the power path during partial shading condition.

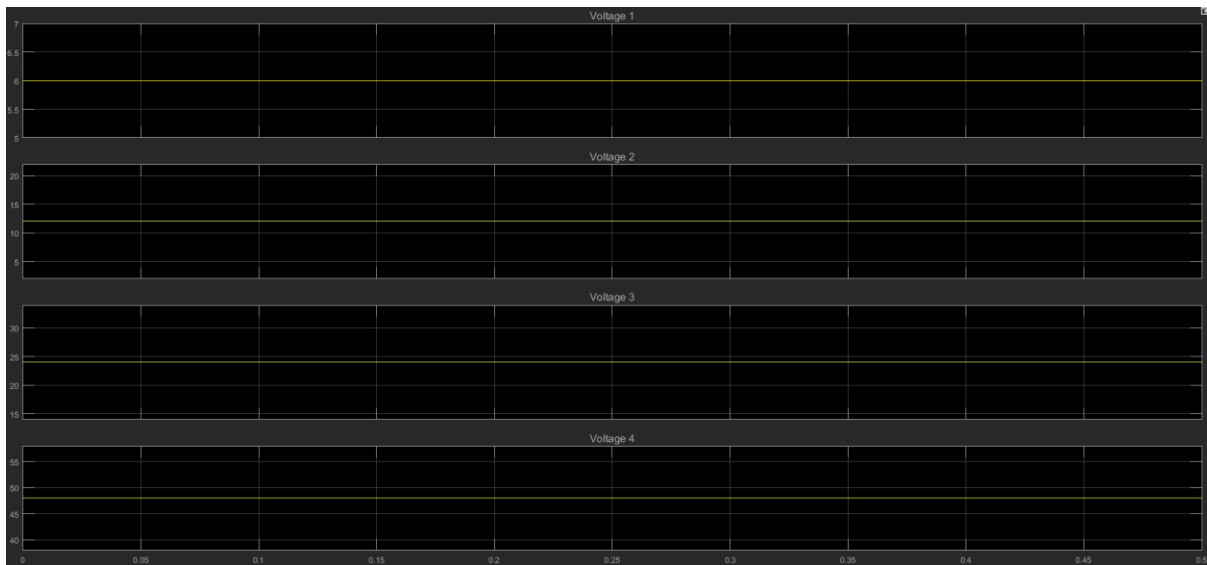


FIGURE 8. Output voltages of the converter (a) V1, (b) V2, (c) V3, and (d) V4.

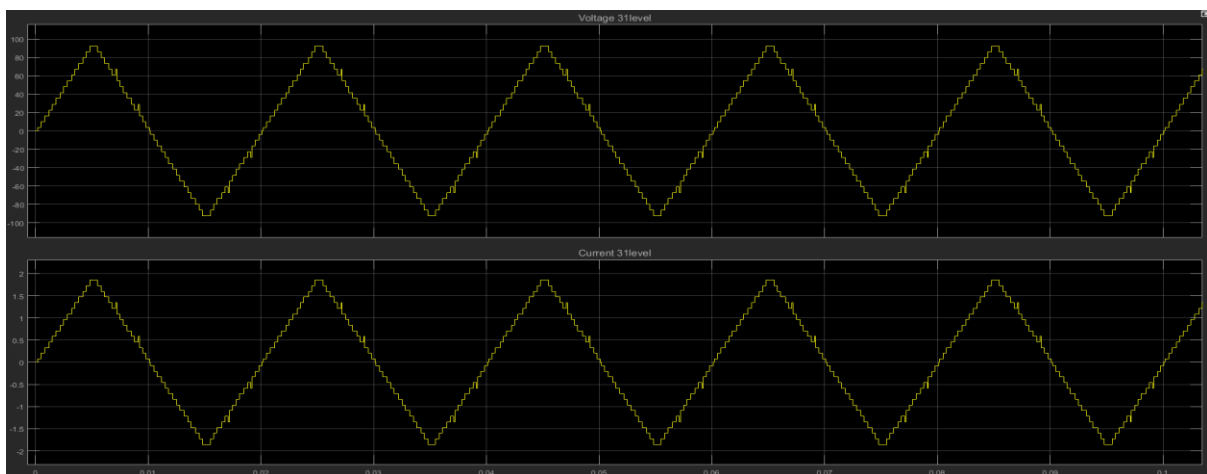
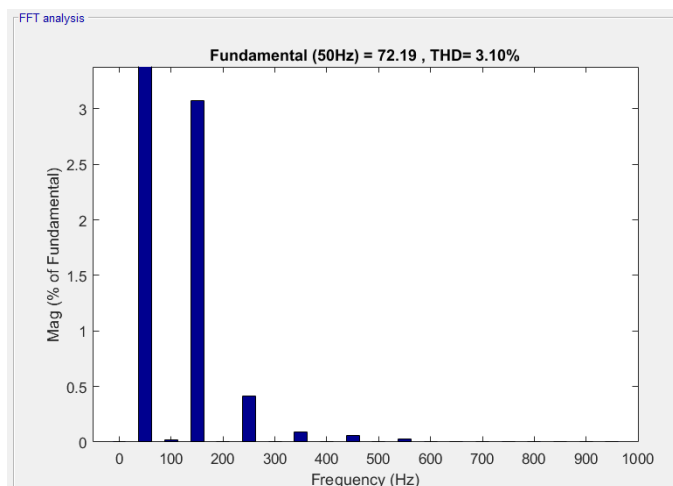


FIGURE 9.



**FIGURE 10.** Output (a) voltage, (b) current, and (c) voltage THD of thirty-one level inverter.

A dc-dc intermediate boost converter is employed to maintain constant output voltage across the PV system. The PV system output voltage is fed to the SIMO converter, which divides the input voltage into four independent voltages. The magnitude of SIMO converter output voltages depends on the turns ratio incorporated in the converter. In this case SIMO converter output voltages are 6V, 12V, 24V and 48V as shown in Fig. 6(a)-(d). In continuation SIMO converter output voltages are given to the MLI. The MLI consists of diode configuration and full bridge converter. The individual DC voltages obtained are inverted into AC voltage. The results plotted in Fig. 7(a) and (b) shows that the inverter output voltage and current are having thirtyone levels, hence resemble a sinusoidal waveform and their respective THD results are depicted in Fig. 7(c). The ripples in the voltage given to the inverter are eliminated by SIMO converter.

#### 4. CONCLUSION

This paper proposes a novel PV inverter topology for solar power generation. The proposed topology consists of a new MPPT scheme based on shading pattern identification using ANFIS, DC-DC single input and multiple output power converter and a simple multi-level inverter with the reduced number of switches. The proposed MPPT scheme is succeeded in harvesting maximum solar power in any weather conditions. The PV voltage is fed to SIMO converter, where PV voltage is segregated into four individual voltages with different magnitudes. Multilevel inverter accepts the four DC voltages as input and thereafter converts it into AC voltage with a minimum voltage and current harmonic distortion of 3.10%. It is worth to mention that the proposed topology extracts maximum power from PV array in any weather conditions and feed the utility at low cost.

#### REFERENCES

- [1]. F. Liu, S. Duan, F. Liu, B. Liu, and Y. Kang, "A variable step size INC MPPT method for PV systems," *IEEE Trans. Ind. Electron.*, vol. 55, no. 7, pp. 2622–2628, Jul. 2008.
- [2]. Q. Mei, M. Shan, L. Liu, and J. M. Guerrero, "A novel improved variable step-size incremental-resistance MPPT method for PV systems," *IEEE Trans. Ind. Electron.*, vol. 58, no. 6, pp. 2427–2434, Jun. 2011.
- [3]. F.-S. Pai and R.-M. Chao, "A new algorithm to photovoltaic power point tracking problems with quadratic maximization," *IEEE Trans. Energy Convers.*, vol. 25, no. 1, pp. 262–264, Mar. 2010.
- [4]. M. A. Elgendy, B. Zahawi, and D. J. Atkinson, "Assessment of perturb and observe MPPT algorithm implementation techniques for PV pumping applications," *IEEE Trans. Sustainable Energy*, vol. 3, no. 1, pp. 21–33, Jan. 2012.
- [5]. E. Mamarelis, G. Petrone, and G. Spagnuolo, "A two-steps algorithm improving the P&O steady state MPPT efficiency," *Appl. Energy*, vol. 113, pp. 414–421, Jan. 2014.
- [6]. K. L. Lian, J. H. Jhang, and I. S. Tian, "A maximum power point tracking method based on perturb-and-observe combined with particle swarm optimization," *IEEE J. Photovolt.*, vol. 4, no. 2, pp. 626–633, Mar. 2014.
- [7]. M. Killi and S. Samanta, "Modified perturb and observe MPPT algorithm for drift avoidance in photovoltaic systems," *IEEE Trans. Ind. Electron.*, vol. 62, no. 9, pp. 5549–5559, Sep. 2015. doi: 10.1109/TIE.2015.2407854.
- [8]. V. R. Kota and M. N. Bhukya, "A simple and efficient MPPT scheme for PV module using 2-dimensional lookup table," in *Proc. IEEE Power Energy Conf. Illinois (PECI)*, Feb. 2016, pp. 1–7, doi: 10.1109/PECI.2016.7459226.
- [9]. L. Zhang, K. Sun, Y. Xing, and J. Zhao, "A family of five-level dualbuck full-bridge inverters for grid-tied applications," *IEEE Trans. Power Electron.*, vol. 31, no. 10, pp. 7029–7042, Oct. 2016.
- [10]. A. Salem, E. M. Ahmed, M. Orabi, and M. Ahmed, "New three-phase symmetrical multilevel voltage source inverter," *IEEE J. Emerg. Sel. Topics Circuits Syst.*, vol. 5, no. 3, pp. 430–442, Sep. 2015.

- [11].J. Rodriguez, L. Moran, J. Pontt, P. Correa, and C. Silva, "A high-performance vector control of an 11-level inverter," *IEEE Trans. Ind. Electron.*, vol. 50, no. 1, pp. 80–85, Feb. 2003.
- [12].G. Graditi, G. Adinolfi, and G. M. Tina, "Photovoltaic optimizer boost converters: Temperature influence and electro-thermal design," *Appl. Energy*, vol. 115, pp. 140–150, Feb. 2014.
- [13].M. R. Airineni and S. Keerthipati, "DC offset minimisation of three-phase multilevel inverter configuration under fault and DC link voltage unbalance conditions," *IET Power Electron.*, vol. 11, no. 2, pp. 293–301, 2018.
- [14].L. He and C. Cheng, "A bridge modular switched-capacitor-based multilevel inverter with optimized spwm control method and enhanced power-decoupling ability," *IEEE Trans. Ind. Electron.*, vol. 65, no. 8, pp. 6140–6149, Aug. 2018.
- [15].M. K. Das, K. C. Jana, and A. Sinha, "Performance evaluation of an asymmetrical reduced switched multi-level inverter for a grid-connected PV system," *IET Renew. Power Gener.*, vol. 12, no. 2, pp. 252–263, 2018.
- [16].A. N. Kumle, S. H. Fathi, F. Jabbarvaziri, M. Jamshidi, and S. S. H. Yazdi, "Application of memetic algorithm for selective harmonic elimination in multi-level inverters," *IET Power Electron.*, vol. 8, no. 9, pp. 1733–1739, 2015.
- [17].R. Agrawal and S. Jain, "Multilevel inverter for interfacing renewable energy sources with low/medium- and high-voltage grids," *IET Renew. Power Gener.*, vol. 11, no. 14, pp. 1822–1831, 2017.
- [18].A. Gaikwad and P. A. Arbune, "Study of cascaded H-Bridge multilevel inverter," in *Proc. Int. Conf. Autom. Control Dyn. Optim. Techn. (ICACDOT)*, 2016, pp. 179–182.
- [19].C. K. Lee, S. Y. R. Hui, and H. S.-H. Chung, "A 31-level cascade inverter for power applications," *IEEE Trans. Ind. Electron.*, vol. 49, no. 3, pp. 613–617, Jan. 2002.
- [20].G. Adinolfi, G. Graditi, P. Siano, and A. Piccolo, "Multiobjective optimal design of photovoltaic synchronous boost converters assessing efficiency, reliability, and cost savings," *IEEE Trans. Ind. Informat.*, vol. 11, no. 5, pp. 1038–1048, Oct. 2015. doi: 10.1109/TII.2015.2462805.